Dominant scattering channel induced by two-body collision of *D*-band atoms in a triangular optical lattice

Xinxin Guo,[1] Zhongcheng Yu,[1] Peng Peng,[1] Guoling Yin,[2,3] Shengjie Jin,[1] Xuzong Chen,[1] and Xiaoji Zhou[1,3,*]

[1]*State Key Laboratory of Advanced Optical Communication Systems and Networks, Department of Electronics, Peking University, Beijing 100871, China*

[2]*State Key Laboratory of Quantum Optics and Quantum Optics Devices, Institute of Opto-Electronics, Shanxi University, Taiyuan 030006, China*

[3]*Collaborative Innovation Center of Extreme Optics, Shanxi University, Taiyuan, Shanxi 030006, China*

(Received 23 May 2021; revised 7 September 2021; accepted 8 September 2021; published 30 September 2021)

The mechanism of atomic collisions in excited bands plays an important role in both the atomic dynamics in high bands of optical lattices and the simulation of condensed matter physics. Atoms distributed in an excited band of an optical lattice can collide and decay to other bands through different scattering channels. In the excited bands of a one-dimensional lattice there is no significant difference between the cross sections to different scattering channels, due to the sameness of all of the geometrical couplings. Here, we investigate the collisional scattering channels for atoms in the excited bands of a triangular optical lattice and demonstrate a dominant scattering channel in the experiment. A shortcut method is utilized to load Bose-Einstein condensate of ^{87}Rb atoms into the Γ point of the first *D* band with zero quasimomentum in the triangular optical lattice. After some evolution time, the number of atoms scattering into the *S* band induced by two-body collisions is around four times the number that scatter into the second most populated band. Our numerical calculation shows that the *ss* scattering channel is dominant, which is roughly consistent with the experimental measurement. The appearance of dominant scattering channels in a triangular optical lattice is owing to nonorthogonal lattice vectors. This work is helpful for the research on many-body systems and directional enhancement in optical lattices.

DOI: 10.1103/PhysRevA.104.033326

I. INTRODUCTION

In many-body systems, collision is one of the most important interactions. The investigations of low-energy collisions in atomic [1–8], ionic [9,10], and electronic systems [11–13] have been a subject of intense research in recent years. As for ultracold atoms, the collision rate is one of the major factors to determine the coherence time of the system [14,15]. The scattering cross section is defined to describe the collision rate, which has been extensively studied experimentally and theoretically [16,17].

The research on ultracold atoms in optical lattices has attracted much attention for their abundant properties especially in excited bands of lattice, including dynamical superfluidity in higher lattice orbitals [18–22], staggered orbital currents [23], and decay mechanisms in excited bands [24,25]. The collision in optical lattices not only changes the internal state of atoms [26,27] but also influences the external state [24]. For instance, two atoms on an excited band in the optical lattice would jump to other bands owing to two-body collision [28]. The path for atoms scattering from a certain initial state to a final state is defined as a scattering channel. So far, several theoretical and experimental works have investigated the effect of atomic collisions in one-, two-, and mixed-dimensional optical lattices [29–33], such as the measurement of the collision rate for atoms in the *P* band [33] and the observation of scattering halos [34], etc. Recently, we have demonstrated the cross section of excited bands in one-dimensional (1D) lattice experimentally [35], where the cross sections to each band have no significant difference and no dominant scattering channel exists. Different from the situation in 1D lattice, two-dimensional (2D) lattice has more information on geometry and dimension, whereas the study of scattering channels in 2D optical lattice has remained unexplored systematically.

Here, we perform theoretical and experimental studies of scattering channels induced by two-body collisions at the Γ point of the first *D* band (D_1 band) in a triangular optical lattice and demonstrate a dominant scattering channel. Our experiment starts from a Bose-Einstein condensate (BEC) in a harmonic trap, and then we use the shortcut method [36] to load the atoms into the Γ point of the D_1 band in the triangular optical lattice. After holding the atoms for a certain time in the optical lattice, we apply a band mapping technique to get the distribution of atoms in reciprocal space [20,37]. We quantitatively measure the number of atoms in different bands through the absorption images obtained after time of flight. We find that 55.8% of atoms jump to the *S* band [the first Brillouin zone (BZ)], while only about 10% of atoms jump to the two *P* bands (second and third BZ, respectively) and about 10% of atoms remain in the D_1 band (fourth BZ). Meanwhile, theoretical calculation indicates that the scattering channel

*xjzhou@pku.edu.cn

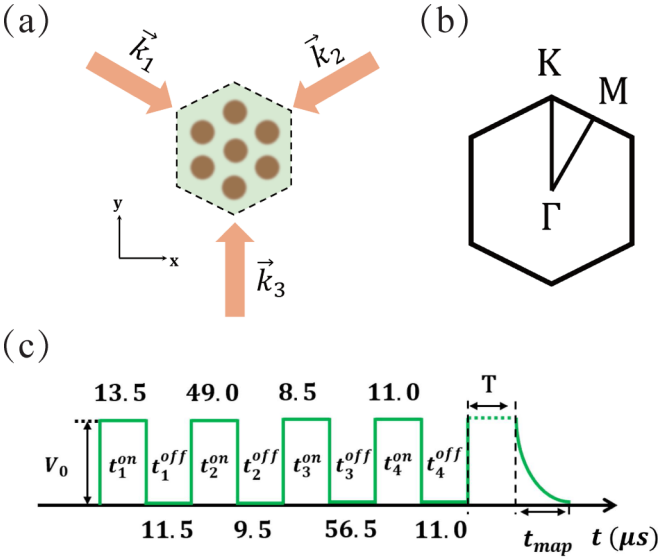

FIG. 1. (a) Diagram of a triangular optical lattice. The arrows represent the laser beams with wave vectors $\vec{k}_i$, where $i = 1$, 2, and 3, and $\vec{k}_3 = -(\vec{k}_1 + \vec{k}_2)$. (b) Reduced Brillouin zone of the triangular lattice corresponding to panel (a). The high symmetry line of the band K-Γ-M-K is marked. (c) The time sequence diagram of the lattice depth for loading atoms into the Γ point of the D_1 band in the triangular lattice. The four pulses $/t_i^{\rm on}/t_i^{\rm off}/$, $i = 1$, 2, 3, and 4, form a shortcut sequence. After an evolution time T, the lattice beam intensity decreases to zero adiabatically in $t_{\rm map} = 1$ ms. The lattice depth of the time sequence is $V_0 = 3.0\ E_r$.

where two atoms jump from the D_1 band to the S band is dominant. By adding up all the scattering channels to the same final state, we get that the cross section to the S band is 57.3% of the total cross section, agreeing with experimental results. The reason for the dominant channel may be nonorthogonal lattice vectors which produce a term of potential affected by both positions x and y and decrease the overlapping area of eigenstates between bands with different parities. This work contributes to the control of external states of atoms in an optical lattice, and the dominant scattering channel is possibly used for realizing directional enhancement.

In Sec. II, we describe the experimental process in the triangular lattice. Section III introduces the collision model and scattering channels in 2D lattice. Then we calculate the cross section of scattering channels in the square and triangular optical lattices, respectively. In Sec. IV, we demonstrate the experimental result and give the normalized scattering cross section of each band. Then we compare the experiments with theoretical calculations. In Sec. V, we compare triangular lattice with bipartite lattices and analyze the connection between lattice geometry and the dominant scattering channel. Finally, we give a conclusion in Sec. VI.

II. EXPERIMENTAL DESCRIPTION

Our experiment is carried out in a 2D triangular optical lattice with tube-shaped lattice sites [19,38–40]. As shown in Fig. 1(a), the triangular optical lattice is formed by three intersecting $\lambda = 1064$-nm laser beams, which are linearly polarized perpendicular to the lattice plane (x-y plane). $\vec{k}_1$, $\vec{k}_2$, and $\vec{k}_3$ are wave vectors of the three laser beams with 120° enclosing angles. In the direction perpendicular to the lattice plane, atoms are weakly confined by an approximately harmonic potential. Figure 1(b) shows the reduced Brillouin zone corresponding to the triangular lattice in Fig. 1(a), and it marks the high-symmetry line K-Γ-M-K.

We start with a BEC of about 3×10^5 atoms in the $|F = 2, m_F = +2\rangle$ state, which is confined in a hybrid trap with the harmonic trapping frequencies $(\omega_x, \omega_y, \omega_z) = 2\pi\times(28, 55, 60)$ Hz. Next, a nonadiabatic shortcut method is utilized to load the BEC from the harmonic trap into the Γ point (the quasimomentum $\vec{q} = 0$) of the D_1 band in the triangular optical lattice [18,24,36]. The duration and interval time sequence of the optical pulses for the shortcut is optimized to reach the target state with high fidelity. For the lattice depth $V_0 = 3.0\ E_r$, after optimizing, we get a four-pulse sequence as shown in Fig. 1(c), and the on/off time of the lattice is 13.5/11.5/49.0/9.5/8.5/56.5/11.0/11.0 μs. The theoretical fidelity of the sequence can reach 99.95% (see Appendix B for more details).

After being loaded into the D_1 band, the BEC in the optical lattice evolves for a certain time T. Then, we apply band mapping [20,41] by switching off the lattice potential adiabatically in the form $e^{-t_{\rm map}/\tau}$, where the time constant $\tau = 200\ \mu$s for the total time $t_{\rm map} = 1$ ms, as shown in Fig. 1(c). Atoms populated in the nth band with quasimomentum $\vec{q}$ and energy E can be mapped to some point of the nth Brillouin zone with quasimomentum $\vec{q}$. Finally, we take absorption imaging with the time of flight (TOF) $t_{\rm TOF} = 30$ ms to measure the quasimomentum space distribution of atoms in each band.

III. COLLISIONAL SCATTERING PROCESS AND CALCULATION OF SCATTERING CHANNELS

In the above section, we describe the experimental process and load the atoms into the Γ point of the D_1 band. To study the evolution of atoms, in this section, we discuss the collisional scattering process of atoms in the excited bands of 2D optical lattice and calculate the cross section of the collisional scattering.

A. Collisional scattering process

The potential of 2D lattice $V_{\rm lattice}$ can be expressed as

$$V_{\rm lattice} = V_x\cos(\vec{k}_x\cdot\vec{r}) + V_y\cos(\vec{k}_y\cdot\vec{r}) + \sum_{a,b} V_{ab}\cos[(a\vec{k}_x + b\vec{k}_y)\cdot\vec{r}], \quad (1)$$

where $\vec{k}_x$ and $\vec{k}_y$ are the lattice vectors in the x and y directions, respectively, and $\vec{r}$ is the position vector. V_x, V_y, and V_{ab} are potential energy components in the x, y, and oblique directions, where a and b are any nonzero integers.

The first two terms on the right side of Eq. (1) are independent, whereas the last term is related to both the vector **x** and the vector **y**, defined as the x part, the y part, and the x-y dimensional coupling part, correspondingly. For a 2D lattice, the appearance of the dimensional coupling part is due to the

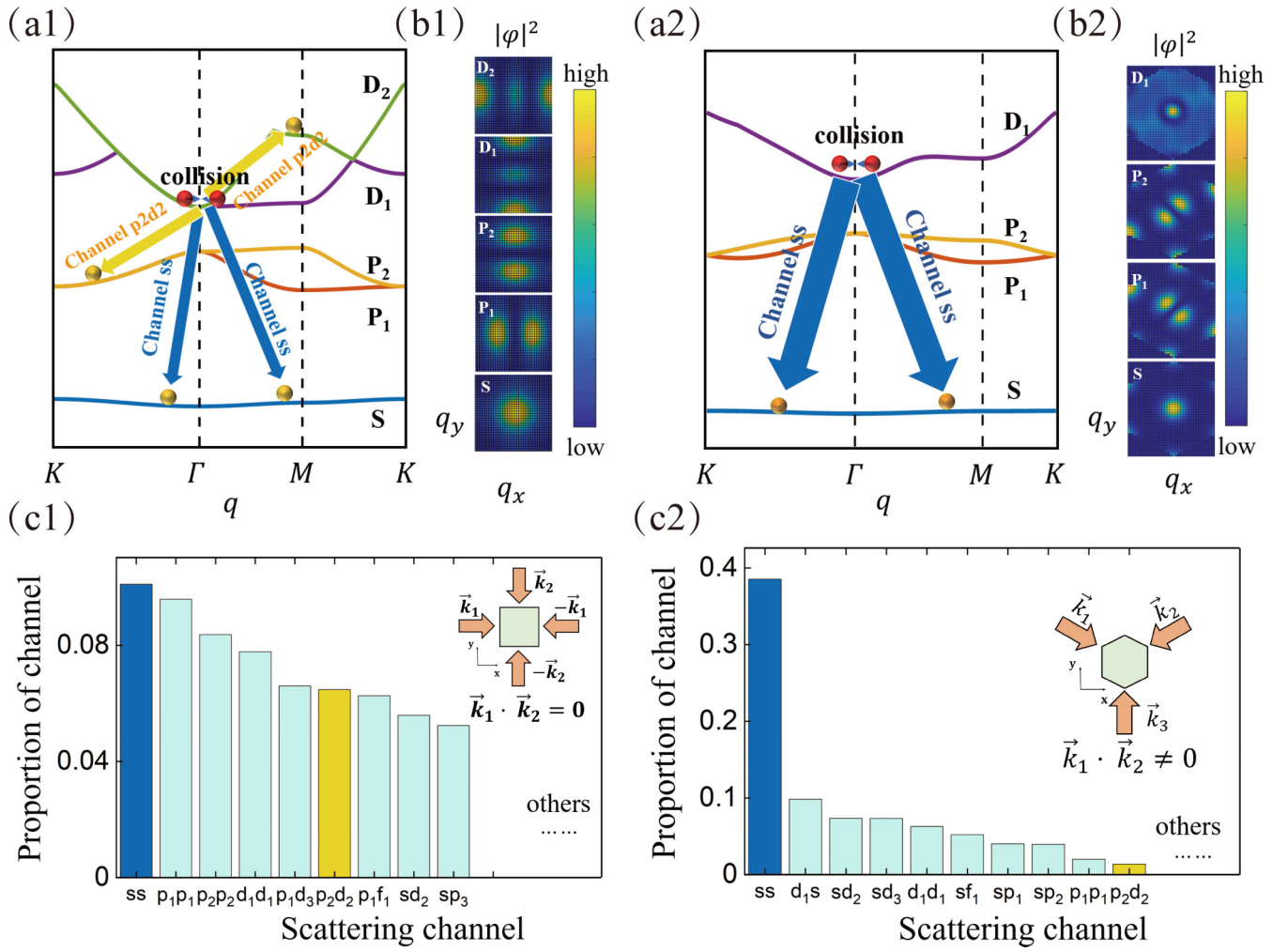

FIG. 2. Scattering channels of atoms in 2D lattice. Panels (a1) and (a2) show the band structure along the high-symmetry lines in square and triangular lattices, respectively. The red and yellow spheres represent the atomic initial states and final states during the collision scattering. Arrows with the same color represent the scattering channel generated by a collision. Here we only draw the first few bands and scattering channels, and others are not shown in the figure. Panels (b1) and (b2) show the squared modulus of the wave function $|u(\vec{q})|^2$ for the states at the Γ points corresponding to bands in panels (a1) and (a2), respectively. The proportions of several main scattering channels are shown in panels (c1) (square lattice) and (c2) (triangular lattice). The inserts show the diagram of a square optical lattice and a triangular optical lattice.

nonorthogonality of lattice vectors. When $V_{ab} = 0$, the lattice potential is independent in the x and y directions, like the square lattice. Comparably, when $V_{ab} \neq 0$, the lattice potential is not independent in the x and y directions, like the triangular optical lattice.

Figures 2(a1) and 2(a2) show the band structure along the high-symmetry line K-Γ-M-K of the square and triangular optical lattices, respectively. For a 2D optical lattice, there are one S band, two P bands (P_1, P_2), and four D bands (D_1, D_2, D_3, D_4). For the ^{87}Rb BEC in the optical lattice, the collisions are mainly low-energy scattering, and the s-wave approximation is reasonable [34]. Further, during the measuring time (about several microseconds), a three-body collision could be neglected, of which the characteristic time is several seconds in the ^{87}Rb BEC. In the following, we just consider a two-body s-wave collision and assume that the atoms only undergo one collision during the scattering process.

As shown in Figs. 2(a1) and 2(a2), atoms initially staying at the Γ point of the D_1 band would jump to other bands because of collisions, where the red and yellow spheres correspond to the initial and final states of the two atoms. As shown by the blue arrows in Figs. 2(a1) and 2(a2), the two atoms both jump to the S band, and we mark this case as the ss scattering channel. Similarly, if one of the two atoms jumps to the P_2 band and another one to the D_2 band, shown as the yellow arrows, it is called the p_2d_2 scattering channel. Different choices of final states are defined as different scattering channels. Briefly, we only draw a few typical scattering channels, and in reality the atoms can jump to any band. However, the probability of scattering to each band is different, and the strength of the scattering probability is defined as the scattering cross section.

B. Calculation of scattering channels

In order to study the difference of the scattering process between a square lattice and a triangular lattice, we use the scattering theory to calculate the cross section of each scattering channel in these two types of lattices. Two-body

collisional scattering cross section for two atoms initially at the Γ point $[(q_x, q_y) = (0, 0)]$ of the D_1 band jumping to bands n_1 and n_2 can be written as [24] (see Appendix A for more details):

$$\sigma(n_1, n_2) = \frac{4\pi m\hbar}{v_a} \int d\vec{q} \times \left| -2\pi i \frac{4\pi a_s}{m} \zeta_{n_1,n_2}(0, 0; \vec{q}, -\vec{q}) \right|^2, \quad (2)$$

where v_a is the atomic velocity, m is the atomic mass, and a_s is the atomic s-wave scattering length. And the overlapping integral of eigenstates $\zeta_{n_1,n_2}(0, 0; \vec{q}, -\vec{q})$ is given by

$$\zeta_{n_1,n_2}(0, 0; \vec{q}, -\vec{q}) = \int d\vec{r} \times u^*_{n_1,\vec{q}}(\vec{r}) u^*_{n_2,-\vec{q}}(\vec{r}) u_{d,0}(\vec{r}) u_{d,0}(\vec{r}), \quad (3)$$

where $u_{n_i,\vec{q}}$ $(i = 1, 2, \ldots)$ is the eigenstate at quasimomentum $\vec{q}$ in band n_i. In the calculation, we assume the periodic boundary conditions, and consider that $|\zeta_{n_1,n_2}(0, 0; \vec{q}, -\vec{q})|^2 = \int d\vec{r} \times |u^*_{n_1,\vec{q}}(\vec{r}) u^*_{n_2,-\vec{q}}(\vec{r}) u_{d,0}(\vec{r}) u_{d,0}(\vec{r})|^2$. Figures 2(b1) and 2(b2) show the modulus square of the eigenstates $u_{n_i,\vec{q}}$ at the Γ point of each band in square and triangular optical lattices, which are calculated by secular equations of the optical lattice, where we choose the wavelength of optical lattice $\lambda = 1064$ nm and the lattice depth $V_0 = 3\, E_r$ ($E_r = \frac{h^2}{2m\lambda^2}$ is the single-photon recoil energy).

To study the proportion of each scattering channel, we consider the lowest seven bands of the square and triangular optical lattices, because the scattering channels of higher bands are weak. Then we calculate the scattering channels, as shown in Figs. 2(c1) and 2(c2). In the square lattice, the cross sections of the strongest channels, ss, p_1p_1, and p_2p_2, are all around 10% of the total cross section, respectively. Besides, there are many other smaller channels included in "Others." There is no significant difference in scattering cross-section values among the first six channels, which means that there is no dominant scattering channel in the square lattice. By contrast, in the triangular lattice, the proportion of the scattering cross section of the ss channel is 38.5%, while that of the second strong channel d_1s is only 9.8%. Besides, the proportions of other channels are much lower than that of the channel ss. Consequently, the channel ss is dominant in the two-body scattering process of the triangular optical lattice.

Further, we study the influence of the lattice depth V_0 on the dominant channel ss in the triangular lattice. Using the same method, we calculate the normalized scattering cross sections of each channel with different lattice depths V_0, as shown in Fig. 3(a). Among those lattice depths, the scattering channel ss is always the dominant scattering channel.

Besides, Eq. (2) can give the differential cross section $\frac{d^2\sigma}{d\vec{q}}(\vec{q})$ of the scattering channel, which denotes the scattering probability to different quasimomenta. Figure 3(b) shows the normalized differential cross section of the channel ss in the triangular optical lattice at $V_0 = 3\, E_r$. The differential cross section covers the entire Brillouin zone, and the value of the differential cross section at the center of the Brillouin zone is 4% lower than that at the edge. Since this difference is small, the atoms would approximately uniformly scatter to the S band, and the 1st BZ almost evenly filled by atoms should be observed.

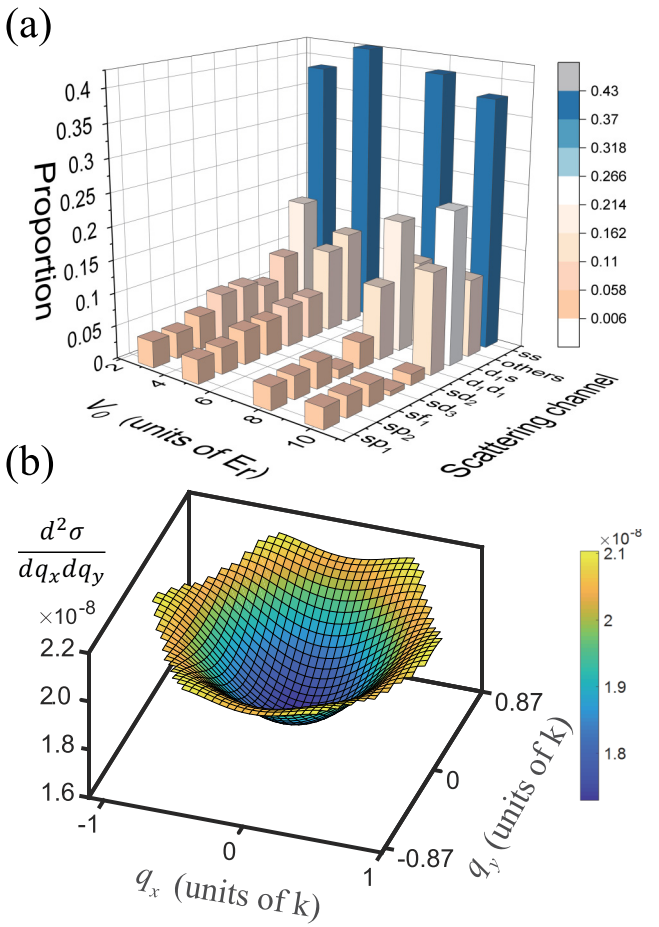

FIG. 3. (a) The proportion of each scattering channel for different lattice depths $V_0 = 3$, 5, 8, and 10 E_r. Several main channels are shown in the figure, and the sum of the proportion of others is shown in "others." (b) Normalized differential cross section of the scattering channel ss with (q_x, q_y) in quasimomentum space, where $k = \frac{2\pi}{\lambda}$.

IV. EXPERIMENTAL RESULTS AND ANALYSIS

A. Experimental results

In the experiment, the distribution of atoms in quasimomentum space could be observed after band mapping. The atomic distribution in the nth band is mapped to the area within the nth Brillouin zone in extended Brillouin zones. Figure 4(a) shows the first four extended Brillouin zones of the triangular lattice, yellow, green, blue, and red areas, corresponding to the S, P_1, P_2, and D_1 bands, respectively. And Fig. 4(b) shows the points with high symmetry, Γ, K, and M, in the 1st and 4th extended Brillouin zones.

Figure 4(c) shows the band population of ultracold atoms, which initially stay at the Γ point of the D_1 band, versus the different evolution times T in the experiment. When $T = 0$ ms, the atoms almost distribute at six points in the 4th Brillouin zone, where there is the Γ point of the D_1 band. As the evolution time T increases, the atoms gradually scatter to other bands. At $T = 1.8$ ms, a considerable number of atoms could be observed in the 1st BZ, while atoms populating in other BZs were few. When $T = 4.0$ ms, the number of atoms at the 1st BZ and the six points of the 4th BZ are close.

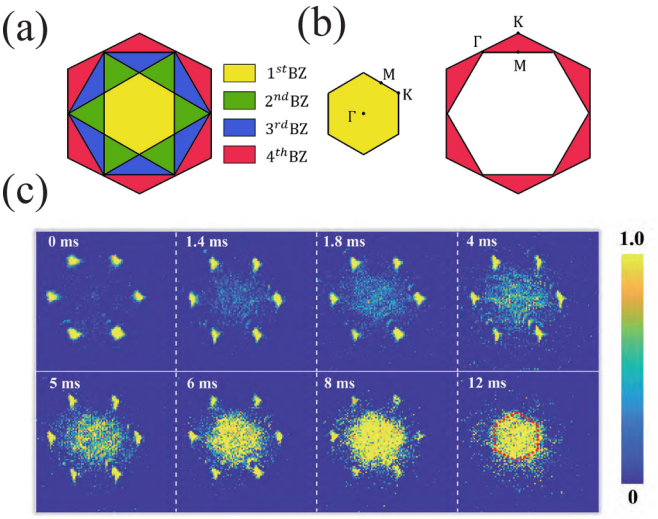

FIG. 4. (a) Schematic diagram of the first four Brillouin zones of a triangular optical lattice. Yellow, green, blue, and red areas represent the 1st, 2nd, 3rd, and 4th BZ, respectively. (b) The position of the high-symmetry point in the 1st and 4th extended Brillouin zone. The yellow area represents the 1st BZ, and the red area represents the 4th BZ. The corresponding positions of points K, Γ, and M in the two areas are marked. (c) Observation of the atomic distribution over different evolution times. A given color represents the same number of atoms in each panel, where the maximum number of atoms is normalized to 1. The red box marks the 1st BZ.

At $T = 8.0$ ms, a prominent part of atoms at the Γ point of the D_1 band decay, and the atoms at the 1st BZ are more numerous than those in any other areas obviously. Finally, at $T = 12.0$ ms, atoms distributed at the Γ point of the D_1 band completely decay, and the 1st BZ is nearly tiled with atoms. The population of atoms in the 1st Brillouin zone forms a hexagon with a clear outline, as the red box marks, agreeing with the calculation of the differential cross section shown in Fig. 3(b).

B. Comparision between experiments and theoretical calculation

To quantitatively compare the theoretical and experimental scattering cross sections, we calculate the proportion of atoms in each Brillouin zone of Fig. 4(c). We define the proportion of atoms in each Brillouin zone as

$$p_i = N_i/N_0, \tag{4}$$

where $i = S, P_1, P_2$, and D_1, and N_i is the number of atoms in band i. N_0 is the total number of atoms.

The proportion of atoms corresponding to Fig. 4(c) is shown in Fig. 5, where Fig. 5(a) shows the proportion of atoms in the D_1 band and Fig. 5(b) shows the proportion of atoms in the S, P_1, P_2, and other higher bands. The error bar of each data point represents the standard deviation of five times measurement. The insert of Fig. 5(a) shows our division of atomic distribution. The six red rectangles mark the Γ point of the D_1 band, and the number of atoms in those areas is considered as N_{D_1}. The yellow lines mark the 1st, 2nd, and 3rd BZs, and the numbers of atoms in these three BZs (except

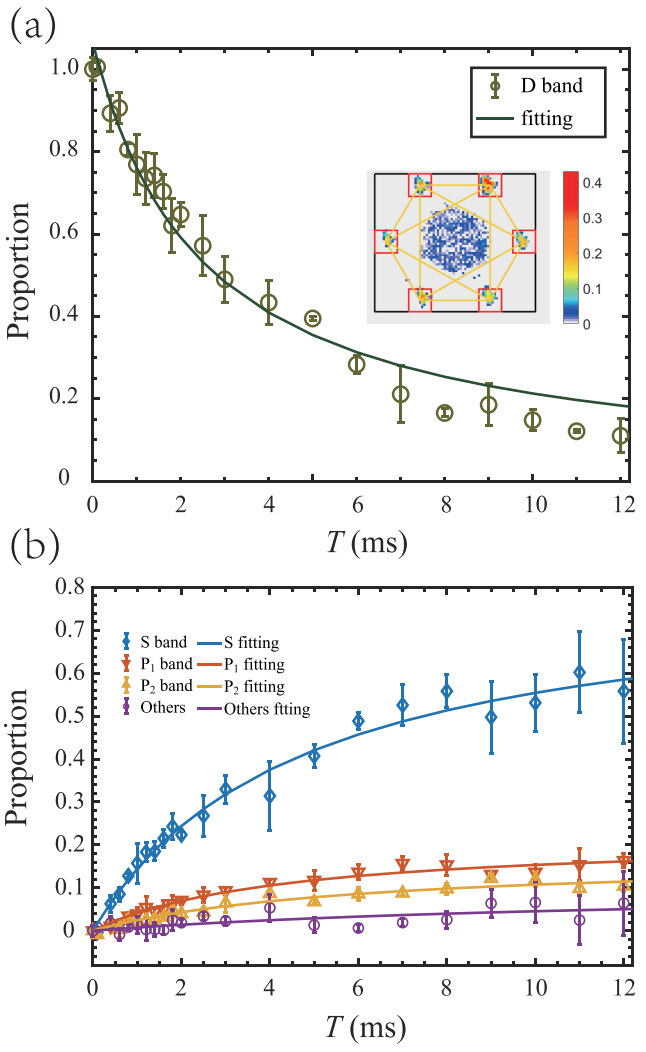

FIG. 5. The normalized proportion of atoms over different evolution times. The proportion of the D_1 band over the evolution time is shown in panel (a), and the proportion of other bands is shown in panel (b). The green circles in panel (a) denote the atomic proportion in the D_1 band and the blue diamonds (orange down triangles, yellow up triangles, and purple circles) in panel (b) represent the atomic proportion in the S band (P_1 and P_2 bands and others), of which the solid lines with the same color are fitting lines. The insert in panel (a) shows the method to extract atom numbers for different Brillouin zones. The error bars represent the standard deviation of the five times measurement. The lattice depth is $V_0 = 3\ E_r$.

the area in the six red rectangles) are defined as N_S, N_{P_1}, and N_{P_2}, respectively. We use the six red rectangles instead of the 4th BZ to make the initial atomic count of the D_1 band more accurate, but it will make the count of atoms at the end of the evolution smaller.

The green hollow circles in Fig. 5(a) show the proportion of atoms at the Γ point of the D_1 band. In Fig. 5(b), the blue (orange and yellow) points indicate the proportion of atoms in the S (P_1 and P_2) band, and the purple points reveal the atoms in other higher bands. The number of atoms in the D_1 band at $T = 0$ ms is defined as the total atom number. The solid lines fit the experimental points by functions $n_0[1 - 1/(1 + KT)]$

[24], where n_0 and K are fitted parameters. At first, the atoms are loaded into the Γ point of the D_1 band. With time increasing, the atoms at the Γ point of the D_1 band gradually scatter to other bands. Hence, the proportion p_{D_1} reduces, while the proportion of atoms in other bands increases. However, the increase rate of p_s is much faster than that of the P_1 and P_2 bands and the others. At $T = 5$ ms, the proportion p_{D_1} reduces to $1/e$. At the same time, p_S raises to 40.7%, and $p_{P_1} = 11.8\%$, $p_{P_2} = 6.7\%$, and $p_{\text{others}} = 1.3\%$. Finally, at $T = 12$ ms, when atoms at the Γ point in the D_1 band almost completely decay, the proportion of atoms in the S band reaches 55.8%, which is nearly four times the number that is in the second highest band, P_1.

In order to connect the scattering channels with the proportion of atoms in each band, we add the scattering channels to the same band and get the theoretical cross section to each band. Taking the cross section of the S band as an example, the cross section is equal to twice the proportion of the channel ss plus the proportion of the channels sp_1, sp_2, sd_1, and so on. Figure 6(a) shows the final proportions of different bands obtained in experiments (orange bars) and the normalized theoretical cross sections (green bars). The theoretical proportion of atoms scattering to the S band is 57.3%, which is roughly consistent with that of the experiment point, 55.8%. Further, the proportion of atoms in other bands is much lower than that in S band both in experiment and theory, indicating that the scattering channel ss is indeed dominant. Besides, we attribute the higher population of the $P_1(P_2)$ band in the experiment than that in the theory to the background in the absorption imaging and the two or more collisions in the evolution time.

Further, we study the influence of the optical lattice depth V_0 on the dominant scattering channel. Figure 6(b) demonstrates the experimental and theoretical proportions of the final proportion of atoms in the S band at different lattice depths V_0. For the lattice depths $V_0 = 3$, 5, 8, and 10 E_r, the experimental measurements [orange squares in Fig. 6(b)] are 55.8%, 56.2%, 58.3%, and 62.6%, which are close to the theoretical points (green diamonds) 57.3%, 61.0%, 58.3%, and 55.3%, respectively. The dominant scattering channel ss always exists with different lattice depths, which is roughly consistent with theoretical calculations in Fig. 3(a).

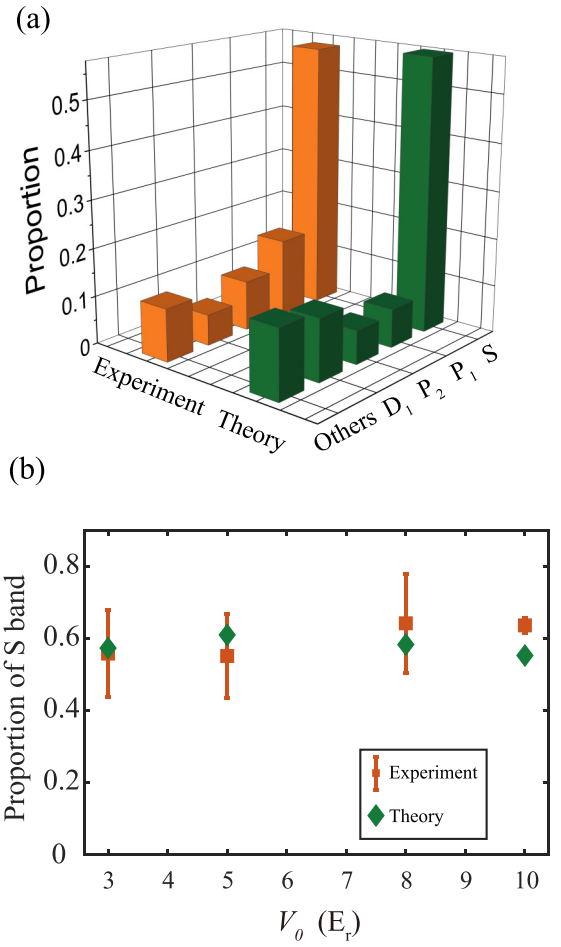

FIG. 6. (a) The proportion of atoms in the S, P_1, P_2, D_1, and other bands, when atoms initially at the Γ point of the D_1 band all decay. The experimental points (orange bars) are consistent with theoretical points (green bars). (b) The proportion of the S band for different lattice depths V_0. Experiment (theory) points are denoted by orange squares (green diamonds). The error bars represent the standard deviation of the five times measurement.

V. SCATTERING CHANNELS IN BIPARTITE LATTICES

Through the above theoretical calculation and experiments, we find that the overlap area of eigenstates between bands with different parities (for example, the D band and the P band) in lattice with nonorthogonal lattice vectors (like triangular lattice) is much smaller than that in lattice with orthogonal lattice vectors (like square lattice). However, the orthogonality of lattice vectors has little effect on the overlapping area between bands with the same parity (for example, the D band and the S band). Hence, in the lattice with nonorthogonal lattice vectors, the scattering channel between bands with the same parity will be dominant.

For an optical lattice potential, the effect of nonorthogonal lattice vectors produces the x-y dimensional coupling term, as shown in Eq. (1). In order to demonstrate the relationship between the lattice geometry and the dominant scattering channels, we calculate the scattering cross sections from the Γ point of the D_1 band in other lattices with or without the x-y dimensional coupling term. In the following calculation, the first seven bands are considered and the lattice depth is $V_0 = 5\,E_r$.

Table I shows the normalized cross section in different lattices. The proportion for the $\bar{S}$ band ($\bar{P}$ band) represents the average proportion for each S band (P band). The proportion for the D_1 band reflects the atoms scattering to the D_1 band. The R_D is defined as

$$R_D = \bar{\mathrm{S}}/\max(\bar{P}, D_1). \tag{5}$$

R_D denotes the ratio of the cross section between the S band and the second biggest band, which indicates whether there exists a dominant scattering channel.

Without the x-y dimensional coupling term, the cross sections in 1D lattice to the S band, the P band, and the D band are similar and the ratio $R_D = 0.50$. Hence, there is no dominant channel, which is also demonstrated in our recent work [35].

TABLE I. The proportion of the scattering cross section in lattice with different geometric structures with $V_0 = 5\ E_r$.

Lattice	$\bar{S}$ band (average)	$\bar{P}$ band (average)	D_1 band	R_D
1D lattice	0.174	0.349	0.300	0.50
Triangular lattice	0.610	0.065	0.142	4.30
Square lattice	0.209	0.207	0.187	1.01
Bipartite square lattice	0.382	0.059	0.050	6.47
Honeycomb lattice	0.317	0.092	0.052	3.45

Square lattice and triangular lattice have been discussed in Sec. II. The lattice vectors of the triangular lattice are nonorthogonal and those of the square lattice are orthogonal. The R_D for the square lattice is 1.01, which indicates there is no dominant scattering channel. In the triangular lattice, the R_D is 4.30, which shows the cross section to the S band is dominant.

Bipartite square lattice and honeycomb lattice are both bipartite lattices, which are easily achieved in experiments by changing the polarizations of beams [40]. The potential of the bipartite lattice is composed of two sets of simple lattice, and the potential of the bipartite square lattice is written as

$$V = V_0\cos(\vec{k}_x\cdot\vec{r}) + V_0\cos(\vec{k}_y\cdot\vec{r}) + V_0\cos[(\vec{k}_x+\vec{k}_y)\cdot\vec{r}] + V_0\cos[(\vec{k}_x-\vec{k}_y)\cdot\vec{r}]. \quad (6)$$

The third and fourth terms of the potential $V_0\cos[(\vec{k}_x+\vec{k}_y)\cdot\vec{r}\,] + V_0\cos[(\vec{k}_x-\vec{k}_y)\cdot\vec{r}\,]$ are x-y dimensional coupling terms. Similarly, honeycomb lattice also has an x-y dimensional coupling term. As shown in Table I, for these two types of lattices, over 30% of atoms scatter to each S band (there are two S bands), while only a few atoms jump to P bands. The R_D of the bipartite square lattice is 6.47, and that of the honeycomb lattice is 3.45, which are both much larger than 1. This indicates that the scattering cross sections to the S bands are dominant in these two types of lattices.

From the calculation, we demonstrate that the scattering channels in lattice without the x-y dimensional coupling term have no significant difference. However, for lattice with the x-y dimensional coupling term, the overlapping areas between bands with different parities are greatly reduced. For example, the ratio of the channel p_1p_1 (ratio of absolute strength) in the triangular lattice to that in the square lattice is 0.29, while the ratio of the channel ss is 0.75. Hence, in lattice with x-y dimensional coupling terms, the decrease of the scattering cross section between energy bands with different parity symmetries is more than that between bands with the same parity symmetry, which induces the channel between the same parity symmetry to be dominant.

VI. CONCLUSION

In conclusion, our experimental measurements and theoretical calculations unveil a dominant scattering channel in the excited bands of triangular optical lattice. After the atoms evolve in the D_1 band of triangular lattice for a certain time, the proportion of atoms scattering to the S band reaches 55.8%, which is around four times the proportion of the second largest band. Our further analysis of the different configuration lattices demonstrates that the x-y dimensional coupling term is the key factor for the dominant scattering channel. This work demonstrates scattering cross sections in 2D optical lattice and paves the way to investigate the collisions in optical lattices, which is important for control of atoms in excited bands. Furthermore, the dominant scattering channel contributes to achieving directional enhancement.

ACKNOWLEDGMENTS

We thank Peng Zhang, Shina Tan, and Xiaopeng Li for helpful discussion. This work is supported by the National Natural Science Foundation of China (Grants No. 61727819, No. 11934002, No. 91736208, and No. 11920101004) and the National Basic Research Program of China (Grant No. 2016YFA0301501).

APPENDIX A: CALCULATION OF SCATTERING CROSS SECTION

We consider the two-body s-wave collision, and we use scattering theory to calculate the scattering cross section. For ^{87}Rb, the higher order of d-wave scattering can be ignored when the temperature is below 200 μK [34]. Hence the s-wave approximation is reasonable for BEC around 80 nK in our experiment.

The incident wave packet can be written as

$$|\Psi_{a,b}\rangle = \int dk_z d\vec{q}_1 d\vec{q}_2 \exp[-i(a\hat{e}_a + b\hat{e}_b)\cdot\vec{K}] \times \phi(\Lambda)|\Lambda, d, d\rangle, \quad (A1)$$

where $\hat{e}_a$ and $\hat{e}_b$ are unit vectors of the cross section. $\Lambda = (k_z, \vec{q}_1, \vec{q}_2)$ and $\vec{K} = [(\vec{q}_1 - \vec{q}_2)/2, k_z]$ are composed of the momentum k_z and the quasimomenta $\vec{q}_1$ and $\vec{q}_2$ of two states. a and b can choose any integer. $\phi(\Lambda)$ is a wave packet, which peaks at Λ. The $|\Lambda, n_1, n_2\rangle$ are eigenstates of two atoms given as

$$|\Lambda, n_1, n_2\rangle = \exp(ik_z z + i\vec{q}_1\cdot\vec{r}_1 + i\vec{q}_2\cdot\vec{r}_2) \times u_{n_1,\vec{q}_1}(\vec{r}_1)u_{n_2,\vec{q}_2}(\vec{r}_2), \quad (A2)$$

where $u_{n_1,\vec{q}_1}(\vec{r}_1)$ and $u_{n_2,\vec{q}_2}(\vec{r}_2)$ are eigenstates of a single atom on n_1 and n_2 bands and are calculated by a secular equation.

According to scattering theory, the scattering cross section of atoms jumping to bands n_1 and n_2 is [24]

$$\sigma(n_1, n_2) = |\hat{e}_a||\hat{e}_b| \sum_{a,b} \int dk_z' d\vec{q}_1' d\vec{q}_2' \times |\langle\Lambda', n_1, n_2|\hat{S} - 1|\Psi_{a,b}\rangle|^2, \quad (A3)$$

TABLE II. The shortcut sequences to load atoms into the Γ point of the D_1 band in the triangular optical lattice with different lattice depths.

V_0	t_1^{on}	t_1^{off}	t_2^{on}	t_2^{off}	t_3^{on}	t_3^{off}	t_4^{on}	t_4^{off} (μs)	Fidelity
3 E_r	13.5	11.5	49.0	9.5	8.5	56.5	11.0	11.0	0.9995
5 E_r	29.5	15.5	16.5	29.5	6.5	31.0	18.0	12.5	0.996
8 E_r	10.5	24.5	18.5	13.0	10.5	55.5	12.5	10.0	0.993
10 E_r	59.5	2.5	20.5	33.5	12.0	13.0	13.5	6.0	0.975

where Λ' is the parameter of the final state of scattering, and $\hat{S}$ is the scattering operator. Using the Born approximation, the scattering operator $\hat{S}$ can be calculated as follows:

$$\langle \Lambda', n_1, n_2|\hat{S}-1|\Psi_{a,b}\rangle = -2\pi i\delta(E_{\Lambda',n_1,n_2}-E_{\Psi_{a,b}})\langle \Lambda', n_1, n_2|U(\vec{r})|\Psi_{a,b}\rangle, \quad \text{(A4)}$$

where

$$U(\vec{r}) = \frac{4\pi a_s}{m}\delta(\vec{r})\frac{\partial}{\partial r}(\vec{r}\cdot) \quad \text{(A5)}$$

is the interaction operator. For the $F=2$, $m_F=+2$ ^{87}Rb atoms, the s-wave scattering length $a_s = 90\,a_B$, where a_B is the Bohr radius. We defined the overlapping integral $\zeta_{n_1,n_2}(\vec{q}_1,\vec{q}_2;\vec{q}_1',\vec{q}_2')$ as

$$\zeta_{n_1,n_2}(\vec{q}_1,\vec{q}_2;\vec{q}\,'_1,\vec{q}\,'_2) = \int_{\vec{r}} d\vec{r} \times u^*_{n_1,\vec{q}_1'}(\vec{r})u^*_{n_2,\vec{q}_2'}(\vec{r})u_{d,\vec{q}_1}(\vec{r})u_{d,\vec{q}_2}(\vec{r}), \quad \text{(A6)}$$

where $\vec{q}_1$, $\vec{q}_2$, $\vec{q}\,'_1$, and $\vec{q}\,'_2$ are the quasimomenta of the initial and final states of two atoms.

Using the overlapping integral (A6), Eq. (A4) is simplified as

$$\langle \Lambda', n_1, n_2|\hat{S}-1|\Psi_{a,b}\rangle \propto \zeta_{n_1,n_2}(\vec{q}_1,\vec{q}_2;\vec{q}_1',\vec{q}_2'). \quad \text{(A7)}$$

In our experiment, atoms initially distribute at the Γ point of the D_1 band ($\vec{q}_1=\vec{q}_2=0$). The system obeys the conservation of momentum, and it causes $\vec{q}_1' = -\vec{q}_2' = \vec{q}$. Hence, the scattering cross section

$$\sigma(n_1,n_2) \propto \int d\vec{q}\ |\zeta_{n_1,n_2}(0,0;\vec{q},-\vec{q})|^2. \quad \text{(A8)}$$

We use the periodic boundary approximation and reduce the right side of the above formula to $\int d\vec{q}\int d\vec{r}\times|u^*_{n_1,\vec{q}}(\vec{r})u^*_{n_2,-\vec{q}}(\vec{r})u_{d,0}(\vec{r})u_{d,0}(\vec{r})|^2$. By calculating the overlapping integral, we can get the proportion of each scattering channel and the differential scattering cross section, as shown in Figs. 3(a) and 3(b).

APPENDIX B: SHORTCUT SEQUENCES

Shortcut is a robust method to load BEC from the harmonic trap into the optical lattice. In our previous work [18,24,36], we have used the method to load atoms into the S band and higher bands of 1D or 2D lattice. The basic principle of the shortcut method is that the evolution operators $U_{\vec{k}}(t)$ of momentum states $|\vec{k}\rangle$ are different between the lattice on and off. As shown in Fig. 1(c), after several laser pluses, the final state of atoms is

$$|\psi_f\rangle = \sum_{\vec{k}}\prod_{i=n}^{1} U_{\vec{k}}^{\text{off}}\left(t_i^{\text{off}}\right)U_{\vec{k}}^{\text{on}}\left(t_i^{\text{on}}\right)\times|\vec{k}\rangle, \quad \text{(B1)}$$

where n is the number of pulses, and $U_{\vec{k}}^{\text{on/off}}(t)$ is the evolution operator when the lattice is on/off.

By choosing the number of pulses and pulse length, we can optimize the final state $|\psi_f\rangle$ to aimed state $|\psi_a\rangle$. The fidelity is defined by $|\langle\psi_f|\psi_a\rangle|^2$ to describe the loading efficiency. In the experiment, the optimized sequence has four pluses to load atoms into D_1 band of triangular optical lattice, and the pulse sequences of different lattice depth are shown in Table II.

[1] M. Olshanii, Phys. Rev. Lett. **81**, 938 (1998).
[2] T. Bergeman, M. G. Moore, and M. Olshanii, Phys. Rev. Lett. **91**, 163201 (2003).
[3] H. Konishi, F. Schäfer, S. Ueda, and Y. Takahashi, New J. Phys. **18**, 103009 (2016).
[4] J. Jie, Y. Zhang, and P. Zhang, Phys. Rev. A **93**, 022705 (2016).
[5] J. M. Hutson, M. Beyene, and M. L. González-Martínez, Phys. Rev. Lett. **103**, 163201 (2009).
[6] J. Weiner, V. S. Bagnato, S. Zilio, and P. S. Julienne, Rev. Mod. Phys. **71**, 1 (1999).
[7] F. Kemper, F. Rosicky, and R. Feder, J. Phys. B: At. Mol. Phys. **17**, 3763 (1984).
[8] Z. Li and R. V. Krems, Phys. Rev. A **79**, 050701(R) (2009).
[9] F. H. J. Hall and S. Willitsch, Phys. Rev. Lett. **109**, 233202 (2012).
[10] R. Saito, S. Haze, M. Sasakawa, R. Nakai, M. Raoult, H. Da Silva, O. Dulieu, and T. Mukaiyama, Phys. Rev. A **95**, 032709 (2017).
[11] D. Seitov, K. Nekrasov, A. Y. Kupryazhkin, S. Gupta, and A. Usseinov, Nucl. Instrum. Methods Phys. Res. Sect. B **476**, 26 (2020).
[12] Y. Yu, G. S. Jung, C. Liu, Y. C. Lin, C. M. Rouleau, M. Yoon, G. Eres, G. Duscher, K. Xiao, S. Irle *et al.*, ACS Nano **15**, 4504 (2021).
[13] R. Tyrrell, B. De Souza, and P. J. Frawley, Cryst. Growth Des. **18**, 617 (2018).

[14] J. P. Burke, J. L. Bohn, B. D. Esry, and C. H. Greene, Phys. Rev. A **55**, R2511 (1997).
[15] C. Chin, R. Grimm, P. Julienne, and E. Tiesinga, Rev. Mod. Phys. **82**, 1225 (2010).
[16] P. A. Altin, N. P. Robins, R. Poldy, J. E. Debs, D. Döring, C. Figl, and J. D. Close, Phys. Rev. A **81**, 012713 (2010).
[17] S. B. Papp and C. E. Wieman, Phys. Rev. Lett. **97**, 180404 (2006).
[18] L. Niu, S. Jin, X. Chen, X. Li, and X. Zhou, Phys. Rev. Lett. **121**, 265301 (2018).
[19] S. Jin, W. Zhang, X. Guo, X. Chen, X. Zhou, and X. Li, Phys. Rev. Lett. **126**, 035301 (2021).
[20] T. Müller, S. Fölling, A. Widera, and I. Bloch, Phys. Rev. Lett. **99**, 200405 (2007).
[21] M. Ölschläger, G. Wirth, and A. Hemmerich, Phys. Rev. Lett. **106**, 015302 (2011).
[22] Z. Wang, B. Yang, D. Hu, X. Chen, H. Xiong, B. Wu, and X. Zhou, Phys. Rev. A **94**, 033624 (2016).
[23] W. V. Liu and C. Wu, Phys. Rev. A **74**, 013607 (2006).
[24] Y. Zhai, X. Yue, Y. Wu, X. Chen, P. Zhang, and X. Zhou, Phys. Rev. A **87**, 063638 (2013).
[25] D. Hu, L. Niu, S. Jin, X. Chen, G. Dong, J. Schmiedmayer, and X. Zhou, Commun. Phys. **1**, 29 (2018).
[26] A. Collin, J. Larson, and J. P. Martikainen, Phys. Rev. A **81**, 023605 (2010).
[27] R. Zhang and P. Zhang, Phys. Rev. A **101**, 013636 (2020).
[28] D. Chen, C. Meldgin, and B. DeMarco, Phys. Rev. A **90**, 013602 (2014).
[29] A. Isacsson and S. M. Girvin, Phys. Rev. A **72**, 053604 (2005).
[30] X. Li and W. V. Liu, Rep. Prog. Phys. **79**, 116401 (2016).
[31] S. Paul and E. Tiesinga, Phys. Rev. A **88**, 033615 (2013).
[32] G. Lamporesi, J. Catani, G. Barontini, Y. Nishida, M. Inguscio, and F. Minardi, Phys. Rev. Lett. **104**, 153202 (2010).
[33] F. Pinheiro, G. M. Bruun, J.-P. Martikainen, and J. Larson, Phys. Rev. Lett. **111**, 205302 (2013).
[34] G. Chatelain, N. Dupont, M. Arnal, V. Brunaud, J. Billy, B. Peaudecerf, P. Schlagheck, and D. Guéry-Odelin, New J. Phys. **22**, 123032 (2020).
[35] H. Shui, S. Jin, Z. Li, F. Wei, X. Chen, X. Li, and X. Zhou, arXiv:2104.08794.
[36] X. Zhou, S. Jin, and J. Schmiedmayer, New J. Phys. **20**, 055005 (2018).
[37] M. Köhl, H. Moritz, T. Stöferle, K. Günter, and T. Esslinger, Phys. Rev. Lett. **94**, 080403 (2005).
[38] C. Becker, P. Soltan-Panahi, J. Kronjäger, S. Dörscher, K. Bongs, and K. Sengstock, New J. Phys. **12**, 065025 (2010).
[39] X. Guo, W. Zhang, Z. Li, H. Shui, X. Chen, and X. Zhou, Opt. Express **27**, 27786 (2019).
[40] S. Jin, X. Guo, P. Peng, X. Chen, X. Li, and X. Zhou, New J. Phys. **21**, 073015 (2019).
[41] I. B. Spielman, P. R. Johnson, J. H. Huckans, C. D. Fertig, S. L. Rolston, W. D. Phillips, and J. V. Porto, Phys. Rev. A **73**, 020702(R) (2006).